Monthly Notices
of the
ROYAL ASTRONOMICAL SOCIETY

MNRAS **453,** 4102–4111 (2015) doi:10.1093/mnras/stv1916

On the central abundances of active galactic nuclei and star-forming galaxies

O. L. Dors Jr,[1⋆] M. V. Cardaci,[2,3⋆] G. F. Hägele,[2,3⋆] I. Rodrigues,[1] E. K. Grebel,[4] L. S. Pilyugin,[4,5,6] P. Freitas-Lemes[1] and A. C. Krabbe[1]

[1] *Universidade do Vale do Paraíba, Av. Shishima Hifumi, 2911, Cep 12244-000, São José dos Campos, SP, Brazil*
[2] *Instituto de Astrofísica de La Plata (CONICET-UNLP), Argentina*
[3] *Facultad de Ciencias Astronómicas y Geofísicas, Universidad Nacional de La Plata, Paseo del Bosque s/n, 1900 La Plata, Argentina*
[4] *Astronomisches Rechen-Institut, Zentrum für Astronomie der Universität Heidelberg, Mönchhofstraße 12-14, D-69120 Heidelberg, Germany*
[5] *Main Astronomical Observatory of National Academy of Sciences of Ukraine, 27 Zabolotnogo str., UA-03680 Kiev, Ukraine*
[6] *Kazan Federal University, 18 Kremlyovskaya St, 420008, Kazan, Russia*

Accepted 2015 August 18. Received 2015 July 22; in original form 2014 December 30

ABSTRACT

We examine the relation between oxygen abundances in the narrow-line regions (NLRs) of active galactic nuclei (AGNs) estimated from the optical emission lines through the strong-line method, via the direct T_e-method, and the central intersect abundances in the host galaxies determined from the radial abundance gradients. We found that the T_e-method underestimates the oxygen abundances by up to ∼2 dex (with averaged value of ∼0.8 dex) compared to the abundances derived through the strong-line method. This confirms the existence of the so-called 'temperature problem' in AGNs. We also found that the abundances in the centres of galaxies obtained from their spectra trough the strong-line method are close to or slightly lower than the central intersect abundances estimated from the radial abundance gradient both in AGNs and star-forming galaxies. The oxygen abundance of the NLR is usually lower than the maximum attainable abundance in galaxies (∼2 times the solar value). This suggests that there is no extraordinary chemical enrichment of the NLRs of AGNs.

Key words: galaxies: abundances – galaxies: evolution – galaxies: formation – galaxies: general – galaxies: ISM.

1 INTRODUCTION

Active galactic nuclei (AGNs) and star-forming regions show prominent emission lines of heavy elements that can be easily measured, even for objects at large redshifts. The intensity of these emission lines depends on the metallicity, which makes them convenient tracers of the chemical evolution of the Universe.

The abundance of a given element in AGNs and in star-forming regions can be derived from measurements of the relative strengths of the emission lines of its ions and of the electron temperature and density of the gas (Osterbrock & Ferland 2006). Oxygen has been generally used as tracer of the metallicity (Z) of star-forming regions (e.g. Tremonti et al. 2004; Nagao, Maiolino & Marconi 2006a; Thuan, Pilyugin & Zinchenko 2010) and of AGNs (Groves, Heckman & Kauffmann 2006; Izotov et al. 2010, among others). Methods for the abundance determinations in star-forming regions have been discussed in many papers. The consensus is that *bona fide* determinations of Z are only obtained by using the T_e-method (Hägele et al. 2006, 2008). This method is based on the determination of the electron temperature (T_e) from the ratios between intensities of two emission lines originating in transitions from two levels with different excitation energies of the same ion, such as the ratios [O III](λ4959+λ5007)/λ4363, [S III](λ9069+λ9532)/λ6312, and [N II](λ6548+λ6584)/λ5755 (see Osterbrock & Ferland 2006.) Unfortunately, these line ratios cannot easily be measured in distant objects and/or in objects with low excitation (e.g. Bresolin et al. 2005), preventing the use of the T_e-method.

Therefore, the oxygen abundances in H II regions are usually estimated using the strong-line method pioneered by Pagel et al. (1979) and Alloin et al. (1979). The principal idea of the strong-line method is to establish the relation between the (oxygen) abundance in an H II region and some combination of the intensities of strong emission lines in its spectrum, i.e. the position of the objects in the strong-line diagram is calibrated in terms of abundance. Therefore, such a relation is often called a 'calibration'. The calibrations of strong emission lines in terms of the oxygen abundances can be

⋆ E-mail: olidors@univap.br (OLDJ); mvcardaci@gmail.com (MVC); guille.h1@gmail.com (GFH)

accomplished by three methods: (i) theoretical calibrations based on photoionization models (e.g. Kewley & Dopita 2002; Dors & Copetti 2005; Dors et al. 2011), (ii) empirical calibrations based on H II regions with abundances derived through the T_e-method (Pilyugin 2000, 2001; Pilyugin & Thuan 2005; Pérez-Montero & Contini 2009, among others), and (iii) hybrid calibrations where both photoionization models and H II regions with T_e-based abundances are used as calibration data points (Pettini & Pagel 2004). The metallicity scales produced by these different methods may differ from each other by up 0.7 dex (Kewley & Ellison 2008).

Here, we use the metallicity scale in H II regions defined by the abundances determined through the classical T_e-method. This is because in the T_e-method, the physical conditions in the nebulae, which are essential ingredients in order to calculate the abundance, are derived directly from observations. Otherwise, if the physical conditions and consequently the abundances are derived by models they will be less certain. This is because of the parameters of the model such as the ionizing source, geometry, etc. tend not to be sufficiently realistic (see Viegas 2002; Kennicutt, Bresolin & Garnett 2003; Dors & Copetti 2005).

AGN metallicities are usually estimated through strong-line theoretical calibrations (e.g. Storchi-Bergmann et al. 1998). Even solar or supersolar abundances have been found. Richardson et al. (2014) established a sequence of photoionization models to reproduce the narrow-line regions (NLRs) of AGN spectra and found that models with a metallicity of $1.4\,Z_\odot$ provide the best agreement with the observational data. Groves et al. (2006) used the photoionization models to analyse the emission lines in the spectra of the NLRs from the Sloan Digital Sky Survey (SDSS; see Tremonti et al. 2004) and found supersolar metallicities for typical Seyfert galaxies (see also Hamann & Ferland 1992, 1993; Ferland et al. 1996; Storchi-Bergmann et al. 1998; Hamann et al. 2002; Baldwin et al. 2003; Dhanda et al. 2007; Wang et al. 2011; Batra & Baldwin 2014; Du et al. 2014). High metallicities at the centres of spiral galaxies are also obtained by the extrapolation of radial abundance gradients to the central regions (Vila-Costas & Edmunds 1992; Zaritsky, Kennicutt & Huchra 1994; van Zee et al. 1998; Pilyugin, Vílchez & Contini 2004; Pilyugin, Thuan & Vílchez 2007; Gusev et al. 2012, among others).

In contrast, low metallicities in AGNs have been obtained when the T_e-method was used (e.g. Zhang, Liang & Hammer 2013). The disagreement between the abundances obtained through the strong-line methods and through the T_e-method is the so-called temperature problem. On the other hand, Izotov & Thuan (2008) determined the abundances through the T_e-method in the AGNs in four dwarf galaxies and found metallicities between 0.05 and 0.2 of the solar value, which is a typical abundance of those galaxies. Alloin et al. (1992), also using the T_e-method, estimated the abundance in the Seyfert 2 (Sy2) nucleus of the galaxy ESO 138 G1 classified as E/S0 (Laubert 1982) and found $Z \approx 0.4\,Z_\odot$. Thus, the T_e-method seems to produce realistic abundance estimations in the low-metallicity range, i.e. the temperature problem seems to disappear at low metallicities. Finding the correct method for the determination of AGN metallicities and establishing a relation between the AGN metallicity and the metallicity of the host galaxy are very important challenges. It should be noted that the AGN metallicity is sometimes adopted as a surrogate metallicity of the host galaxy, mainly at high redshifts (e.g. Nagao, Maiolino & Marconi 2006b; Matsuoka et al. 2009; Dors et al. 2014).

Nowadays, a large number of measured intensities of emission lines sensitive to the electron temperature are available for AGNs in the literature. This also holds for determinations of oxygen gradients in a large sample of spiral galaxies. This provides the possibility for an analysis of the metallicity determinations in AGNs. The main goals of the current study are as follows. (i) To investigate the discrepancy between AGN abundances derived through the strong-line methods and through the T_e-method. The magnitude of this discrepancy is well known for star-forming regions (Pilyugin 2003; Kewley & Ellison 2008; López-Sánchez & Esteban 2010, among others); however, this problem has received less attention in the case of the NLRs of AGNs. (ii) To compare the abundances of the NLRs of AGNs and nuclear star-forming regions estimated from their spectra and central oxygen abundances of the host galaxies derived from the radial abundance gradients. Differences between these values could be evidence in favour of the existence of gas infall on to the centre of a galaxy or extraordinary chemical enrichment of these objects.

The present study is organized as follows. In Section 2, we compare the NLR abundances determined through the T_e-method and the strong emission-line relations of Storchi-Bergmann et al. (1998, hereafter SB98). We examine the relation between the abundances in the NLRs estimated from their optical emission-line spectra and the central intersect abundances in the host galaxies determined from the radial abundance gradients in Section 3. The conclusions are given in Section 4.

2 ABUNDANCE DETERMINATIONS IN NLRs: T_E-METHOD VERSUS RELATIONS BY SB98

2.1 AGN sample

Intensities of narrow emission lines of AGNs were compiled from the literature. Our selection criterion was the presence of flux measurements of the narrow optical emission lines [O II] λ3727, [O III] λ4363, H β, [O III] λ5007, H α, [N II] λ6584, and [S II] λλ6717,6731. We only considered galaxies whose nuclei were classified as Sy2 and Sy1.9. Sequences of photoionization models, not including the shock gas but only a power-law radiation of the ionizing source, are able to reproduce measurements of strong narrow emission lines of Sy2 and Sy1.9 for a large spectral range (e.g. Groves et al. 2006; Dors et al. 2012; Riffel et al. 2013a). Hence, the selection of these AGN types minimizes the effects of shock gas excitations and ionizations, which are not considered in our abundance determinations.

We list in Table 1 the identification of the objects, the emission-line intensities (relative to H β=1.0), the spectral classification taken from the NED,[1] and bibliographic references from which the data were taken. The sample consists of 47 local AGNs (redshift $z < 0.1$) observed with long-slit spectroscopy. In the cases where the reddening correction was not performed in the original works (indicated in Table 1), we dereddened the emission lines comparing the observed H α/H β ratio with the theoretical value of 2.86 (Hummer & Storey 1997), obtained for an electron temperature of 10 000 K and an electron density of $100\,cm^{-3}$.

The emission-line flux errors are reported in the original works for only 4 out of the 47 objects of our sample. Therefore, the errors are not given in Table 1. Typical errors of the emission-line

[1] The NASA/IPAC Extragalactic Database (NED) is operated by the Jet Propulsion Laboratory, California Institute of Technology, under contract with the National Aeronautics and Space Administration.

Table 1. Emission-line intensities of AGNs relative to H β=1.00 compiled from the literature.

Object	[O II] λ3727	[O III] λ4363	[O III] λ4959	[O III] λ5007	H α	[N II] λ6584	[S II] λ6717	[S II] λ6731	Type	Ref.
NGC 7674	1.29	0.12	3.94	12.55	3.70	3.68	0.54	0.64	Sy2	1
IZw 92	2.63	0.32	3.52	10.12	2.42	0.97	0.37	0.40	Sy2	1
NGC 3393[a, b]	2.41	0.14	5.47	16.42	2.78	4.50	0.64	0.89	Sy2	2
Mrk 176	3.54	0.32	4.69	14.36	2.81	2.99	0.56	0.54	Sy2	3
3c33	4.93	0.32	4.10	12.68	2.63	1.76	0.87	0.73	Sy2	3
Mrk 3	3.52	0.24	3.99	12.67	3.10	3.18	0.73	0.82	Sy2	3
NGC 1068	1.23	0.22	4.11	12.42	2.57	4.55	0.26	0.55	Sy2	3
Mrk 573	2.92	0.18	3.89	12.12	2.95	2.47	0.75	0.80	Sy2	3
Mrk 78	4.96	0.14	3.88	11.94	2.46	2.32	0.68	0.61	Sy2	3
Mrk 34	3.43	0.15	3.68	11.46	2.99	2.18	0.82	0.80	Sy2	3
Mrk 1	2.78	0.21	3.56	10.95	2.66	2.21	0.49	0.52	Sy2	3
3c433	6.17	0.41	3.27	9.44	3.38	5.13	1.58	1.13	Sy2	3
Mrk 270	5.64	0.28	2.96	8.71	3.14	2.93	1.21	1.39	Sy2	3
3c452	4.81	0.18	2.40	6.85	2.98	3.58	1.10	0.77	Sy2	3
Mrk 198	2.51	0.12	1.79	5.56	3.02	2.26	0.89	0.68	Sy2	3
Mrk 268	3.75	0.25	1.55	4.82	3.38	4.94	1.28	1.08	Sy2	3
Mrk 273	8.27	0.22	1.52	4.44	2.94	2.62	0.89	0.54	Sy2	3
NGC 3227[b]	3.22	0.50	3.57	10.73	2.86	5.01	1.24	1.26	Sy2	4
Mrk 6	2.45	0.28	3.37	10.13	2.79	1.79	0.62	0.63	Sy2	4
ESO 138 G1	2.35	0.34	2.93	8.71	3.01	0.68	0.47	0.48	Sy2	5
NGC 5643[a, b]	5.55	0.54	4.20	12.61	2.66	2.90	0.91	0.71	Sy2	6
NGC 1667	11.50	0.59	2.78	9.20	2.80	6.96	1.37	1.17	Sy2	7
Mrk 423	8.00	0.40	2.80	6.20	2.90	3.60	1.20	1.00	Sy1.9	8
Mrk 609	1.80	0.50	1.80	5.00	2.80	2.60	0.60	0.50	Sy1.9	8
Mrk 226SW	5.23	0.08	1.50	4.50	3.35	2.07	0.29	0.25	Sy2	9
NGC 3081[a]	2.16	0.23	4.53	12.62	2.73	2.33	0.60	0.62	Sy2	10
NGC 3281[a]	2.33	0.22	2.77	7.59	2.64	2.54	0.53	0.60	Sy2	10
NGC 3982[a]	3.92	0.03	5.64	18.68	2.76	2.57	0.76	0.82	Sy2	10
NGC 4388[a]	2.68	0.15	3.67	10.63	2.71	1.44	0.68	0.60	Sy2	10
NGC 5135[a]	2.01	0.10	1.40	4.47	2.64	2.35	0.37	0.35	Sy2	10
NGC 5643[a]	5.11	0.42	4.56	15.4	2.64	3.07	0.97	0.90	Sy2	10
NGC 5728[a]	3.41	0.44	3.70	10.98	2.65	3.71	0.41	0.41	Sy2	10
NGC 6300[a]	15.48	1.39	8.32	23.32	2.59	6.62	1.42	1.26	Sy2	10
NGC 6890[a]	2.77	0.72	7.48	20.05	2.75	4.26	0.65	0.52	Sy2	10
IC 5063[a]	5.06	0.28	3.37	10.31	2.77	2.67	0.69	0.60	Sy2	10
IC 5135[a]	4.05	0.25	2.07	6.88	2.65	3.30	0.49	0.46	Sy2	10
Mrk 744	2.38	0.33	3.18	8.84	2.47	3.62	2.83	2.83	Sy2	11
Mrk 1066	3.34	0.08	1.22	3.84	2.76	2.42	0.51	0.55	Sy2	11
NGC 5506	2.84	0.14	2.46	7.69	2.84	2.53	0.92	0.99	Sy1.9	12
NGC 2110	4.38	0.26	1.61	4.76	2.66	3.76	1.52	1.38	Sy2	12
NGC 3281[a, b]	4.30	0.42	2.44	7.34	2.60	2.60	0.78	0.73	Sy2	13
Akn 347[a]	2.98	0.42	4.95	15.01	2.65	3.23	0.75	0.75	Sy2	14
UM 16[a]	2.90	0.22	4.62	14.00	2.72	1.70	0.45	0.45	Sy2	14
Mrk 533[a]	1.59	0.13	4.03	12.23	2.72	2.72	0.39	0.45	Sy2	14
IZw 92[a]	2.60	0.34	3.54	10.14	2.78	1.00	0.40	0.43	Sy2	14
Mrk 612[a]	1.88	0.17	2.99	9.37	2.67	3.60	0.74	0.55	Sy2	14
Mrk 622[a]	10.06	0.03	1.90	5.44	2.47	2.33	0.19	0.14	Sy2	14

References – (1) Kraemer et al. (1994), (2) Contini (2012), (3) Koski (1978), (4) Cohen (1983), (5) Alloin et al. (1992), (6) Schmitt, Storchi-Bergmann & Baldwin (1994), (7) Radovich & Rafanelli (1996), (8) Osterbrock (1981), (9) Osterbrock & Dahari (1983), (10) Phillips, Charles & Baldwin (1983), (11) Goodrich & Osterbrock (1983), (12) Shuder (1980), (13) Durret & Bergeron (1988), and (14) Shuder & Osterbrock (1981).

Notes. [(a)]Data corrected for reddening in this work.

[(b)]Value of I[O III] λ4959 estimated from the theoretical relation I[O III] λ4959=I[O III] λ5007/3.0.

intensities are about 10–20 per cent (e.g. Kraemer et al. 1994), which yield uncertainties in the oxygen abundance estimations of about 0.1–0.2 dex (e.g. Kennicutt et al. 2003; Hägele et al. 2008; Dors et al. 2011; Rosa et al. 2014). Hereafter, we will assume that the oxygen estimations from the T_e-method and the relations by SB98 have an uncertainty of 0.15 dex, an average of the values above. For the objects for which the flux of the line [O III] λ4959 is not available, this was calculated from the theoretical relation I[O III] λ4959=I[O III] λ5007/3.0.

2.2 Relations of SB98

SB98 carried out NLR model calculations using the photoionization code CLOUDY (Ferland et al. 1996) and suggested two relations for the abundance determinations in the NLRs of AGNs. The first one is

$$\begin{aligned}(\mathrm{O/H})_{\mathrm{SB98,1}} = {} & 8.34 + (0.212\,x) - (0.012\,x^2) - (0.02\,y) \\ & + (0.007\,xy) - (0.002\,x^2y) + (6.52\times10^{-4}\,y^2) \\ & + (2.27\times10^{-4}\,xy^2) + (8.87\times10^{-5}\,x^2y^2), \end{aligned} \quad (1)$$

where $x = [\mathrm{N\,II}]\,\lambda\lambda6548,6584/\mathrm{H}\,\alpha$ and $y = [\mathrm{O\,III}]\,\lambda\lambda4959,5007/\mathrm{H}\,\beta$. The second relation of SB98 is

$$\begin{aligned}(\mathrm{O/H})_{\mathrm{SB98,2}} &= 8.643 - 0.275\,u + 0.164\,u^2 \\ &+ 0.655\,v - 0.154\,uv - 0.021\,u^2v \\ &+ 0.288v^2 + 0.162uv^2 + 0.0353u^2v^2, \end{aligned} \quad (2)$$

where $u = \log([\mathrm{O\,II}]\ \lambda\lambda3727,3729/[\mathrm{O\,III}]\ \lambda\lambda4959,5007)$ and $v = \log([\mathrm{N\,II}]\ \lambda\lambda6548,6584/\mathrm{H}\ \alpha)$. Both calibrations are valid for $8.4 \leqq 12 + \log(\mathrm{O/H}) \leqq 9.4$.

The dependence of these relations on the density should be taken into account. This dependence is given by the expression considered by SB98:

$$(\mathrm{O/H})_{\mathrm{final}} = \mathrm{O/H} - 0.1\ \log(N_\mathrm{e}/300), \quad (3)$$

where N_e is the electron density in cm^{-3} and the correction is valid for $100\ \mathrm{cm}^{-3} \lesssim N_\mathrm{e} \lesssim 10^4\ \mathrm{cm}^{-3}$. It should be noted that the value of this correction exceeds 0.1 dex for high-density objects only, i.e. for objects with electron densities $N_\mathrm{e} \gtrsim 3{\times}10^3\ \mathrm{cm}^{-3}$.

2.3 T_e-method

We use the emission-line intensities listed in Table 1 to determine the oxygen abundances $(\mathrm{O/H})_{T_\mathrm{e}}$ of the NLRs through the classic T_e-method. We will follow the methodology described in Dors et al. (2013) based on the equations given by Pérez-Montero & Contini (2009), Hägele et al. (2008), Pérez-Montero et al. (2007), and Pérez-Montero & Díaz (2003).

The electron temperature in the high-ionization zone (referred to as t_3) for each object was obtained from the observed line-intensity ratio R_{O3}=[O III](λ4959 + λ5007)/λ4363 using the expression

$$t_3 = 0.8254 - 0.000\,2415\,R_{\mathrm{O3}} + \frac{47.77}{R_{\mathrm{O3}}}, \quad (4)$$

with t_3 in units of 10^4 K. The electron temperature of the low-ionization zone (referred to as t_2) was derived from the theoretical relation:

$$t_2^{-1} = 0.693\,t_3^{-1} + 0.281. \quad (5)$$

The O^{++} and O^{+} ionic abundances were computed through the relations:

$$\begin{aligned}12 + \log\left(\frac{\mathrm{O}^{++}}{\mathrm{H}^{+}}\right) &= \log\left(\frac{I(4959) + I(5007)}{I(\mathrm{H}\,\beta)}\right) + 6.144 \\ &+ \frac{1.251}{t_3} - 0.55\log t_3, \end{aligned} \quad (6)$$

and

$$\begin{aligned}12 + \log\left(\frac{\mathrm{O}^{+}}{\mathrm{H}^{+}}\right) &= \log\left(\frac{I(3727)}{I(\mathrm{H}\,\beta)}\right) + 5.992 \\ &+ \frac{1.583}{t_2} - 0.681\log t_2 + \log(1 + 2.3n_\mathrm{e}). \end{aligned} \quad (7)$$

Finally, we assumed

$$\frac{\mathrm{O}}{\mathrm{H}} = \frac{\mathrm{O}^{+}}{\mathrm{H}^{+}} + \frac{\mathrm{O}^{++}}{\mathrm{H}^{+}} \quad (8)$$

for the determination of the total abundance.

2.4 Abundance results

Electron densities (N_e), O III electron temperatures (T_e), and the oxygen abundances estimated using three different ways for the objects in our sample are reported in Table 2. The oxygen abundances of some objects cannot be determined through the relations given by SB98 because for those objects the estimated abundances or electron densities are outside of the validity ranges considered by these authors, i.e. beyond of the range of values for which the relations are defined. The electron densities, N_e, for the objects in our sample were computed from the line-intensity ratio [S II] λ6716/λ6731

Table 2. Object name, electron density, electron temperature, and oxygen abundance obtained via the T_e-method and via the calibrations of Storchi-Bergmann et al. (1998, equations 1 and 2) for the objects in our sample. Oxygen abundance value estimations outside the validity interval of the calibrations were not considered.

			12+log(O/H)		
Object	N_e (cm^{-3})	T_e (10^4 K)	T_e-method	SB98,1	SB98,2
NGC 7674	1148.0	1.14	8.49	8.72	9.19
IZw 92	822.0	1.95	7.90	8.44	8.67
NGC 3393	2022.0	1.09	8.69	–	9.24
Mrk 176	535.0	1.61	8.21	8.84	9.02
3c33	252.0	1.72	8.14	8.64	8.80
Mrk 3	948.0	1.49	8.26	8.75	8.96
NGC 1068	26 993.0	1.44	8.40	–	–
Mrk 573	781.0	1.34	8.33	8.65	8.92
Mrk 78	370.0	1.22	8.49	8.74	8.88
Mrk 34	546.0	1.27	8.39	8.61	8.85
Mrk 1	767.0	1.50	8.17	8.63	8.90
3c433	50.0	2.38	7.84	8.96	9.04
Mrk 270	1027.0	1.97	7.99	8.62	8.75
3c452	50.0	1.76	7.95	8.80	8.95
Mrk 198	111.0	1.59	7.88	8.61	8.84
Mrk 268	260.0	2.68	7.52	8.76	8.93
Mrk 273	50.0	2.60	7.73	8.67	8.72
NGC 3227	647.0	2.49	7.75	8.98	9.15
Mrk 6	647.0	1.81	7.95	8.55	8.84
ESO 138 G1	685.0	2.22	7.73	8.40	8.53
NGC 5643	141.0	2.36	7.90	8.86	8.96
NGC 1667	281.0	3.12	7.84	9.15	9.06
Mrk 423	239.0	3.14	7.67	8.73	8.80
Mrk 609	239.0	4.41	7.11	8.62	8.92
Mrk 226SW	296.0	1.45	8.08	8.52	8.60
NGC 3081	693.0	1.84	7.85	8.60	8.91
NGC 3281	974.0	1.86	7.84	8.61	8.90
NGC 3982	819.0	0.68	9.54	8.87	8.99
NGC 4388	343	1.31	8.30	8.54	8.80
NGC 5135	492.0	1.61	7.78	8.57	8.83
NGC 5643	451.0	1.79	8.17	8.93	8.99
NGC 5728	606.0	2.26	7.84	8.86	9.05
NGC 6300	360.0	2.96	8.11	–	9.17
NGC 6890	176.0	2.11	8.06	–	9.35
IC 5063	311.0	1.79	8.06	8.51	8.65
IC 5135	471.0	2.12	7.78	8.72	8.90
Mrk 744	606.0	2.16	7.76	8.83	9.10
Mrk 1066	839.0	1.56	7.90	8.54	8.69
NGC 5506	809.0	1.46	8.09	8.60	8.85
NGC 2110	395.0	2.78	7.54	8.73	8.87
NGC 3281	471.0	2.87	7.61	8.66	8.83
Akn 347	606.0	1.82	8.09	8.93	9.11
UM 16	606.0	1.37	8.35	8.59	8.87
Mrk 533	1046.0	1.18	8.44	8.72	9.12
IZw 92	805.0	2.02	7.87	8.42	8.65
Mrk 612	75.0	1.46	8.10	8.89	9.24
Mrk 622	64.0	0.97	8.76	8.69	8.73

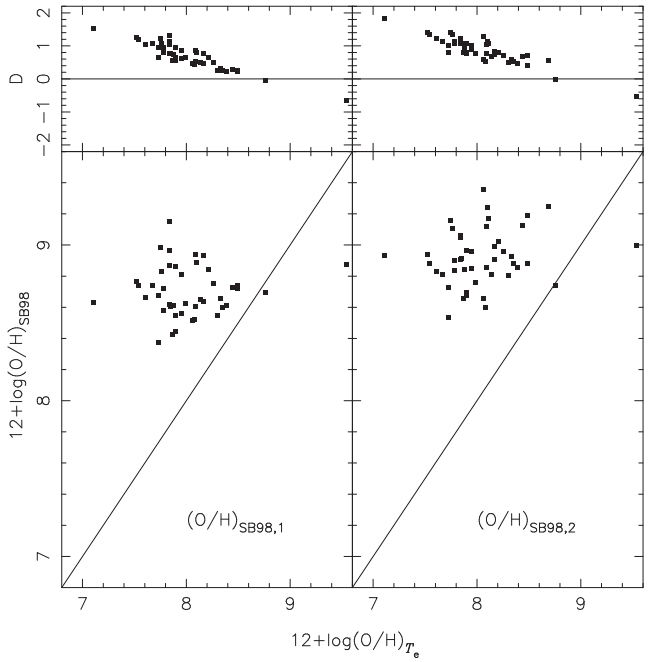

Figure 1. The bottom panel shows the comparison between the oxygen abundance obtained through the T_e-method and through the two calibrations of SB98 as indicated in each plot. The upper panel shows the differences between those O/H estimations.

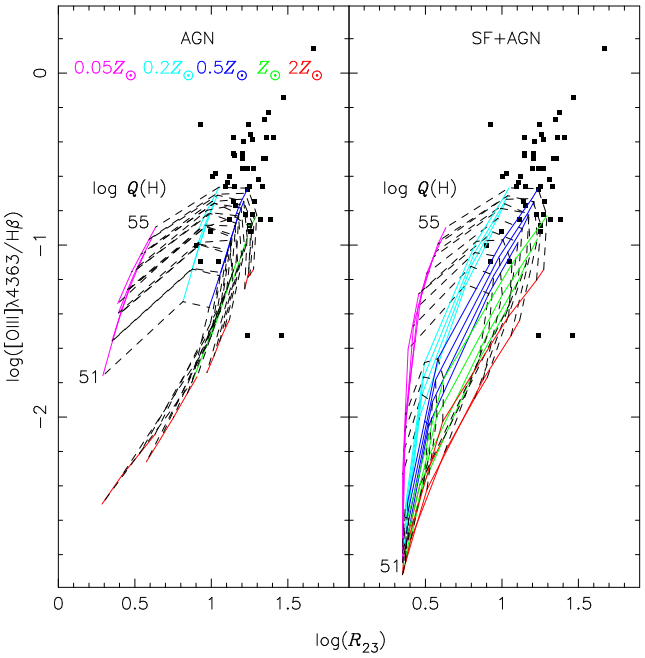

Figure 2. The [O III] λ4363/H β line ratio as a function of the $R_{23} = [I([\mathrm{O\,II}]\lambda3727) + I([\mathrm{O\,III}]\lambda4959 + \lambda5007)]/I(\mathrm{H}\beta)$ parameter. The left-hand panel shows the predictions of the AGN model. The predictions of SF+AGN model are plotted in right-hand panel. The points are the objects of our sample (see Table 1). The typical error (error bars not shown) of the emission-line ratios is about 10 per cent. The solid lines connect the predictions of the models with the same metallicity Z, while dashed lines connect models with the same ionizing photon number (Q(H)).

using the TEMDEN routine of the nebular package of IRAF.[2] Most of our objects have values in the range $0.01 < n_e < 0.12$, where $n_e = N_e/(10^4\ \mathrm{cm}^{-3})$. These values are somewhat higher than the ones derived for H II regions, which were found to be $n_e < 0.06$ (see Copetti et al. 2000; Krabbe et al. 2014). However, they are sufficiently low so that one does not need to consider the contribution from the collisional de-excitation (Rubin 1989) or the direct recombination of the forbidden lines used in the standard abundance determinations.

We found the electron temperature t_3 to be in the range of 6 000–50 000 K, with an average value of ∼20 000 K. This value is somewhat higher than the one found by Zhang et al. (2013) for Sy2s, who used data from SDSS DR7 and found an average value of 14 000 K.

Fig. 1 shows the comparison between oxygen abundances in NLRs determined through the two methods presented above. Inspection of Fig. 1 reveals that the T_e-method provides oxygen abundances lower than the ones obtained via the relations of SB98 by up to ∼2 dex, with an average value of ∼0.8 dex, which confirms the existence of the so-called temperature problem in AGNs. This discrepancy is much larger than the one found for H II regions. For example, Kennicutt et al. (2003), using spectroscopy data of H II regions in spiral galaxies, found that O/H abundances computed from relations based on photoionization models of Kewley & Dopita (2002) are higher by 0.2–0.5 dex than the ones from the T_e-method.

The abundance discrepancy in AGNs could be caused by the presence of a secondary heating (ionizing) source in addition to the radiation from the gas accretion on to the AGN. This secondary source is probably related to the shock. Indeed, Zhang et al. (2013) showed that the strong [O III] λ4363 flux in AGNs (and consequently high electron temperature) suggests the presence of some supplementary energy source(s), which could be due to the presence of shock waves (see also Prieto, Marco & Gallimore 2005; Contini 2012). Moreover, the presence of fluctuations of electron temperature (Peimbert 1967) in the gas phase of AGNs could also contribute for the discrepancies found in Fig. 1.

In order to examine if Sy2 galaxies have a secondary heating source, we performed a simple test. In Fig. 2, the intensity of [O III] λ4363/H β versus the R_{23} parameter defined as $R_{23} = [I([\mathrm{O\,II}]\lambda3727) + I([\mathrm{O\,III}]\lambda4959 + \lambda5007)]/I(\mathrm{H}\beta)$ for the objects in our sample and the ones predicted by a grid of photoionization models are shown.

We consider two models to reproduce the observational data: (i) the AGN model to describe the NRL spectra, and (ii) the SF+AGN model to describe composite (star-forming regions + AGN) spectra. We use the version 08.00 of the CLOUDY code (Ferland et al. 1996) to construct NLR models similar to the ones used by Dors et al. (2012), but considering the table-AGN model (Mathews & Ferland 1987) as the ionizing source. We considered a large range of values for the physical parameters: the number of ionizing photons, $51 \leqq \log Q(\mathrm{H}) \leqq 55$; electron densities, $1.0 \leqq \log(N_e) \leqq 4.0$; and metallicities, $0.05 \leqq (Z/Z_\odot) \leqq 2$. The spectrum of the SF+AGN model is the sum of the predictions of the SF model and the AGN model. The SF model is constructed using the CLOUDY code (Ferland et al. 1996) assuming the ionizing source to be a stellar cluster with an age of 2.5 Myr and $\log Q(\mathrm{H}) = 52.85$ whose spectrum is computed with the STARBURST99 code (Leitherer et al. 1999). The metallicity of the gas phase was considered to be solar with an electron density $N_e = 100\,\mathrm{cm}^{-3}$. These parameters are similar to the ones derived in circumnuclear star formation regions

[2] Image Reduction and Analysis Facility, distributed by NOAO, operated by AURA, Inc., under agreement with the NSF.

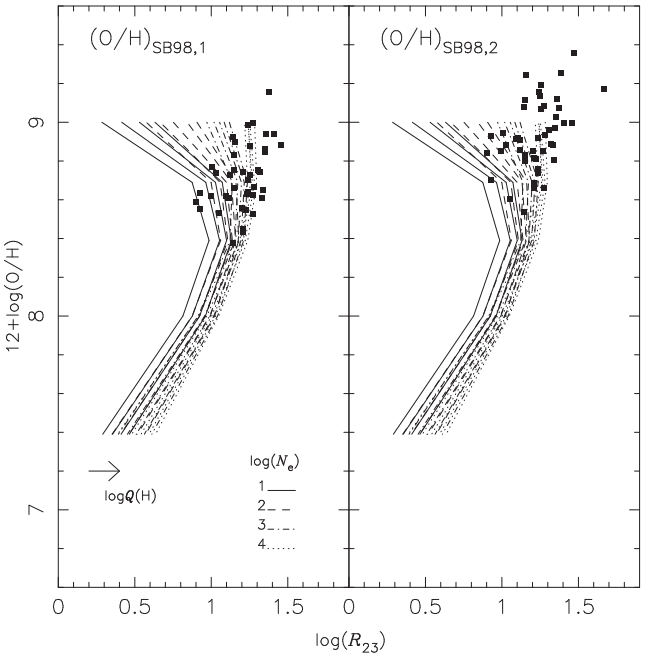

Figure 3. 12+log(O/H) versus log(R_{23}). The points represent oxygen abundances in our objects estimated through the two relations (see Section 2.2) proposed by SB98 as indicated in each plot. Lines show our photoionization model results for different values of electron densities, as indicated, and the logarithm of the ionizing photon numbers (log Q(H)=51–54, with a step of 1 dex). The arrow indicates the direction in which the logarithm of the ionizing photon numbers increases in each model set.

observed in two galaxies (NGC 1097 and NGC 6951) containing a Sy2 nucleus by Dors et al. (2008).

We can see in Fig. 2 that the ratio [O III] λ4363/H β is underpredicted by the AGN and SF+AGN models when compared the observations. This line ratio depends strongly on the electron temperature; therefore, the electron temperatures in AGNs predicted by our models are lower than the ones estimated using the T_e-method. Thus, this discrepancy could be attributed to the presence of gas shock waves propagating at supersonic velocities through the NLRs, which does to enhance the intensity of [O III] λ4363 producing larger electron temperature values and, consequently, low (unrealistic) O/H values when using the T_e-method (see Nagao, Murayama & Taniguchi 2001, and references therein).

Due to the result above, in our paper the T_e-method is no longer used to compute the metallicity of AGNs.

SB98 pointed out that an averaged value of Z obtained from both relations (equations 1 and 2) should be used. Instead of doing that we use our models to choose which of the relations by SB98 yields more reliable abundances. For that, we use the standard O/H–R_{23} empirical diagram. The R_{23} parameter was suggested by Pagel et al. (1979) as indicator of the oxygen abundance when the T_e-method cannot be applied. Although R_{23} has a strong dependence on metallicity, it also depends on the ionization degree of the nebulae, which should be taken into account (Pilyugin 2001, 2000). We compare the predictions of our AGN models with the observed O/H–R_{23} diagram for the objects in our sample, where the oxygen abundances are estimated using both relations of SB98 (see Fig. 3). Since the AGN and SF+AGN models predict similar values of R_{23} in the zone of Fig. 2 where our data are located, only the former models are shown in Fig. 3. In this figure, we can see that a better agreement is obtained when the abundances are determined through the first relation of SB98. Hereafter, this relation will be used.

3 ABUNDANCE AT THE CENTRE OF A GALAXY VERSUS CENTRAL INTERSECT ABUNDANCE

3.1 The data

It is a widely accepted practice to specify the abundance at the centre of a galaxy by the central intersect abundance obtained from the radial abundance gradient (e.g. Vila-Costas & Edmunds 1992; Zaritsky et al. 1994; van Zee et al. 1998; Pilyugin et al. 2004, 2007; Gusev et al. 2012, among others). The radial abundance gradients in the discs of nearby late-type galaxies were recently determined by Pilyugin, Grebel & Kniazev (2014) and Pilyugin, Grebel & Zinchenko (2015). The extrapolation of the radial abundance gradient to the zero galactocentric distance gives the central intersect abundance (O/H)$_0$ in galaxies. On the other hand, Ho, Filippenko & Sargent (1997) obtained emission-line spectra of the central regions of many nearby galaxies. This provides a possibility to estimate the oxygen abundances at the centres of those galaxies. The comparison between central oxygen abundance estimated from the spectrum of the centre of the galaxy with that obtained from the radial abundance gradient can tell us something about the chemical evolution of the central parts of galaxies.

We compare the central O/H abundances estimated from the spectra of Ho et al. (1997) and the central intersect abundances obtained by Pilyugin et al. (2014, 2015). We selected from the sample of Ho et al. (1997) only the galaxies with central spectra classified by Ho et al. (1997) as H II-like regions or Seyferts and which are also in the Pilyugin et al. (2014, 2015) list. Our selected sample contains 45 objects (12 AGNs and 33 star-forming regions) whose emission-line intensities and derived oxygen abundances (see below) are listed in Table 3. Fig. 4 shows the positions of the 45 sample objects in a BPT diagnostic diagram (Baldwin, Phillips & Terlevich 1981), together with a large sample of emission-line SDSS galaxies studied by Thuan et al. (2010), which are plotted with cyan (grey) symbols. In this figure, we also plotted the boundary lines obtained by Kauffmann et al. (2003) and Kewley et al. (2001) that separate the H II-like objects and AGNs in the diagram.

Pilyugin et al. (2014, 2015) derived oxygen abundances from the published emission-line intensities of disc H II regions through the C method (see Pilyugin, Grebel & Mattsson 2012). This is an empirical method based on the comparison between strong emission-line intensities in the spectrum of a target H II region and those in a set of reference H II regions with known abundances. The strong emission lines considered in this method are [O II] λ3727, H β, [O III] λ5007, [N II] λ6584, and [S II] λ6716, λ6731. The optical data of Ho et al. (1997) consist of long-slit spectroscopy of the nuclear region ($r \lesssim 200$ pc) of a large sample of nearby galaxies covering the 4200–5200Å and 6200–6900Å spectral ranges with spectral resolutions of about 4 and 2.5 Å pixel^{-1}, respectively. We use again the first relation of SB98 to estimate the central abundances of the NLRs of the active galaxies [(O/H)$_{\rm SB98,\,1}$]. In the case of galaxies with central H II-like regions, we use the $C_{\rm NS}$ method (Pilyugin et al. 2012, 2013) to estimate the oxygen abundances [(O/H)$_{C_{\rm NS}}$]. The $C_{\rm NS}$ method is a variant of the C method applicable when the [O II] λ3727 emission lines are not available.

Table 3. Dereddened nuclear emission-line fluxes (normalized to the flux of H β=1.00) taken from Ho et al. (1997) and oxygen abundances derived by us. The oxygen abundances 12+log(O/H) for the NLRs of AGNs and central star-forming regions are estimated through the SB98 calibration (equation 1) and through the C_{NS} method, respectively. The values of 12+log(O/H)$_0$ are the central intersect abundances in the galaxies obtained from the radial abundance gradients.

Object	[O III] λ5007	[N II] λ6584	[S II] λ6717+λ6731	12+log(O/H)	12+log(O/H)$_0$
		NLRs of AGNs			
NGC 1058	3.64	3.50	1.95	8.58	8.62
NGC 1068	12.10	2.17	0.68	8.54	8.64
NGC 2336	2.84	5.12	2.99	8.74	8.80
NGC 3031	4.07	6.38	3.89	8.78	8.58
NGC 3227	5.92	3.82	1.95	8.62	8.64
NGC 3486	4.50	3.01	2.64	8.56	8.60
NGC 4258	10.20	2.29	2.61	8.51	8.54
NGC 4395	6.23	0.93	2.04	8.34	8.19
NGC 4501	5.15	6.02	2.66	8.80	8.92
NGC 4725	6.68	3.27	1.82	8.59	8.83
NGC 5033	4.59	6.76	2.99	8.85	8.64
NGC 5194	8.09	8.26	2.28	9.01	8.88
		Nuclear star-forming regions			
NGC 598	1.57	0.48	0.61	8.35	8.48
NGC 783	0.19	1.03	0.55	8.65	8.68
NGC 925	0.81	0.63	0.96	8.41	8.48
NGC 1156	4.51	0.28	0.46	8.24	8.16
NGC 2403	1.91	0.79	1.03	8.36	8.48
NGC 2537	1.84	0.43	0.48	8.35	8.35
NGC 2903	0.08	0.97	0.52	8.71	8.82
NGC 2997	0.31	1.00	0.77	8.56	8.80
NGC 3184	0.12	0.94	0.55	8.67	8.66
NGC 3198	0.23	1.19	0.84	8.59	8.60
NGC 3310	0.91	1.88	0.71	8.55	8.37
NGC 3319	0.99	0.46	1.71	8.26	8.50
NGC 3344	0.83	1.20	1.15	8.49	8.72
NGC 3351	0.25	1.31	0.66	8.62	8.82
NGC 3359	0.54	0.88	1.55	8.43	8.40
NGC 3631	0.29	1.23	0.68	8.60	8.71
NGC 3738	2.99	0.26	0.81	8.13	8.10
NGC 3893	0.21	1.05	0.61	8.62	8.73
NGC 4088	0.19	0.91	0.48	8.65	8.71
NGC 4214	3.66	0.19	0.33	8.20	8.20
NGC 4254	0.87	1.37	0.59	8.54	8.77
NGC 4303	1.32	2.23	1.12	8.53	8.78
NGC 4449	2.36	0.40	0.65	8.26	8.26
NGC 4490	2.34	0.71	1.89	8.22	8.29
NGC 4535	0.13	1.17	0.61	8.66	8.71
NGC 4559	0.32	1.20	1.10	8.53	8.53
NGC 4631	1.51	0.69	0.63	8.42	8.39
NGC 4654	0.14	0.77	0.60	8.63	8.66
NGC 4656	3.96	0.14	0.50	8.04	8.06
NGC 5248	0.26	1.48	0.64	8.61	8.64
NGC 5457	0.23	1.08	0.70	8.61	8.71
NGC 5474	1.75	0.37	0.72	8.26	8.19
NGC 6946	0.37	1.81	0.81	8.55	8.72

3.2 Abundance at the centre versus central intersect abundance

In the bottom panel of Fig. 5, we show the comparison between the central intersect abundances in the selected galaxies (O/H)$_0$ obtained from the radial abundance gradients and central abundances (O/H)$_{SB98,\,1}$ and (O/H)$_{C_{NS}}$ determined from the spectral measurements of the central regions of Ho et al. (1997). This figure shows that the (O/H)$_{SB98,\,1}$ abundances in the NLRs are close to or slightly lower than the central intersect abundances in the host galaxies. The central abundances in galaxies with central H II-like regions show a similar behaviour. Thus, the metallicity in the NLRs obtained through the relation of SB98 is close to the central metallicity of the host galaxy estimated from the radial abundance gradient. The mean difference (D) between the direct and intersect central oxygen abundances (see the upper panel of Fig. 5) for H II-like objects is -0.11 ± 0.09 at high metallicities (12+log(O/H)>8.5) and 0.00 ± 0.08 at low metallicities (12+log(O/H)<8.5). The mean difference for AGNs is -0.01 ± 0.13 at high metallicities. The differences for the high-metallicity AGNs seem to follow a linear regression with a slope of $-0.32(\pm0.33)$ dex^{-1}. The differences for H II-like objects follow a regression with a slope of $-0.45(\pm0.23)$ dex^{-1} at high metallicities, and with a slope of

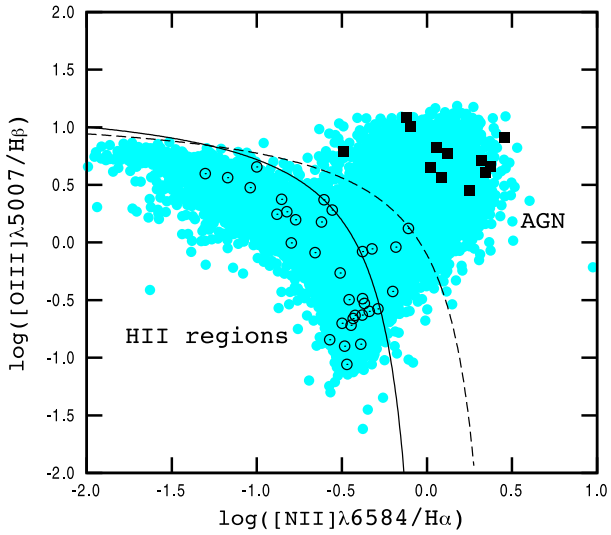

Figure 4. BPT [O III] λ5007/H β versus [N II] λ6584/H α diagnostic diagram. Filled squares and open circles stand for the AGNs and star-forming central regions selected from the work of Ho et al. (1997). Solid and dashed curves mark the boundary between AGNs and H II regions defined by Kauffmann et al. (2003) and Kewley et al. (2001), respectively. The filled circles show a large sample of emission-line SDSS galaxies studied by Thuan et al. (2010).

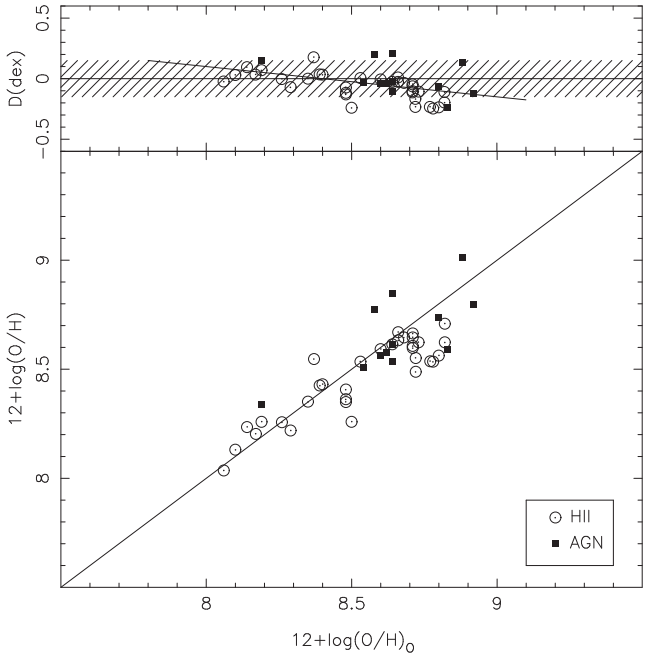

Figure 5. Comparison between central intersect oxygen abundances derived from the radial abundance gradients (O/H)$_0$ and the central abundances determined from the spectra of the central regions from Ho et al. (1997) through the SB98 calibration for the AGNs (filled squares) and through the C_{NS} method for the H II-like regions (open circles). The diagonal line in the bottom panel is the one-to-one relation. The upper panel shows the differences between the spectral and central intersect abundances. The hatched area indicates a band of 0.15 dex adopted for the oxygen abundance uncertainty (see Section 2.1). Solid line shows the linear regression [$D = (-0.25 \pm 0.06) \times 12 + \log(\mathrm{O/H})_0 + 2.10(\pm 0.59)$] considering all data.

$-0.23(\pm 0.15)$ dex^{-1} at low metallicities. We also performed a linear regression considering all points in Fig. 5 due to the small sample we are using. It yields a slope of $-0.25(\pm 0.06)$ dex^{-1}.

The differences are within the uncertainty in the abundance estimations (i.e. compatible with zero). However, the existence of a trend in the differences suggests that the direct central abundance in some high-metallicity galaxies can be lower than the central intersect abundance. It should be noted that Sánchez et al. (2014) have also found observational evidence of lower central oxygen abundances than that predicted by the central abundance extrapolation of the gradients in a number of spiral galaxies. A possible explanation of the trend of the differences with metallicity could be the accretion of metal-poor gas on to the centres of galaxies. In the case of the low-metallicity galaxies, where the metallicity of the accretion material is similar (or not so different) to that of the gas in the central region, the infalling gas should not significantly change the local metallicity. In contrast, in the case of high-metallicity galaxies, this low-metallicity infalling gas would dilute the heavy element content of the gas in the central region. Therefore, this effect would be more relevant in high-metallicity galaxies than in low-metallicity ones.

Observational evidence of the presence of gas flows from the outer parts (with low-metal content material) to the centre of the galactic disc (high-metal content) has been found for isolated barred galaxies (Zaritsky et al. 1994; Martin & Roy 1995) and interacting ones (Ellison et al. 2010, 2011; Kewley et al. 2010; Rosa et al. 2014). Likewise, there are several kinematical studies based on optical and infrared integral field spectroscopy that support the scenario where gas is infalling towards the central region of AGNs (e.g. Fathi, Storchi-Bergmann & Riffel 2006; Storchi-Bergmann et al. 2007; Riffel et al. 2008; Schnorr-Müller et al. 2011, 2014; Riffel, Storchi-Bergmann & Winge 2013b). Moreover, Rupke, Kewley & Barnes (2010) performed numerical simulations of galaxy mergers and found that the central underabundances observed in this kind of systems could be accounted for by a radial infall of low-metallicity material coming from the outskirts of both galaxies involved.

3.3 Is there an extraordinary chemical enrichment of the NLRs?

It was found by Pilyugin, Thuan & Vílchez (2006) and Pilyugin et al. (2007) that there is an upper limit to the oxygen abundances in galaxies, i.e. there is a maximum attainable oxygen abundance. These authors found that this maximum value of oxygen abundance in galaxies is about twice the solar abundance (adopting the solar oxygen abundance to be $12 + \log(\mathrm{O/H})_\odot = 8.69$; Allende Prieto, Lambert & Asplund 2001).

The abundances in the NLRs of AGNs taken from the list of Ho et al. (1997) are in the range $8.5 < 12 + \log(\mathrm{O/H}) < 9.0$ or $0.6 < Z/Z_\odot < 2$, which does not exceed the maximum attainable abundance for galaxies. This suggests that there is no an extraordinary chemical enrichment of the NLRs. Similar AGN abundances were obtained by Matsuoka et al. (2009) from the analysis of the C IV λ1549/He II λ1640–C III] λ1909/C IV λ1549 diagram calibrated in terms of gas abundance through photoionization models using the CLOUDY code (Ferland et al. 1996). Dors et al. (2014) also obtained similar abundances using a new index ($C_{43} = \log[(\mathrm{C\,IV}\lambda 1549 + \mathrm{C\,III}]\lambda 1909)/\mathrm{He\,II}\lambda 1640]$) defined by them as a metallicity indicator for AGNs.

However, it should be noted that we found metallicities larger than twice solar up to $Z/Z_\odot \sim 6.5$ [$12 + \log(\mathrm{O/H})_{\mathrm{SB98,1}} \sim 9.5$ (see Fig. 1]) for five AGNs from Table 1. Similarly extra high

metallicities for some NLRs were obtained by SB98. Further study of the galaxies with possible extra high metallicity AGNs should be carried out (in particular, radial abundance distributions and central intersect abundances should be obtained in those galaxies) in order to be able to draw solid conclusions about the upper limit to the oxygen abundances in NLRs.

4 SUMMARY AND CONCLUSIONS

We compiled from the literature a sample of spectra of NLRs of AGNs with available optical emission lines: [O II] λ3727, [O III] λ4363, H β, [O III] λ5007, H α, [N II] λ6584, [S II] λ6717, and [S II] λ6731. We estimated the oxygen abundances in those NLRs through the classic T_e-method and through the strong-line method (the calibration of Storchi-Bergmann et al. 1998). We found that the abundances determined through the T_e method are lower by up to ∼2 dex than the abundances estimated through the calibration of SB98, i.e. we confirmed the existence of the so-called temperature problem in AGNs.

We also considered a second sample of galaxies for which the emission-line spectra of the central regions were measured by Ho et al. (1997) and the central intersect abundances were found by Pilyugin et al. (2014, 2015). The direct central abundances of the AGNs and star-forming regions in those galaxies were estimated through the calibration of Storchi-Bergmann et al. (1998) and through the C_{NS} method (Pilyugin et al. 2012, 2013), respectively. We found that the abundances of the NLRs and H II-like objects estimated from the direct spectral measurements are close to or slightly lower than the central intersect abundances obtained from the radial abundance gradients. This may suggest that the infall of the low-metallicity gas on to the centres of the galaxies can take place in some galaxies where the central abundance estimated from the direct spectral measurements is lower than the central intersect abundance.

The abundances in the NLRs of the AGNs in our samples do not suggest that there is an extraordinary chemical enrichment of the NLRs. There are only a few AGNs with oxygen abundances higher than the maximum attainable abundance for galaxies (∼2 times the solar value; Pilyugin et al. 2006, 2007). Additional investigations of the galaxies with possible extra high metallicity AGNs are necessary to draw reliable conclusions on the upper limits of the oxygen abundances in NLRs.

ACKNOWLEDGEMENTS

We are grateful to the anonymous referee for his/her useful comments and suggestions that helped us to substantially clarify and improve the manuscript. OLD and ACK are grateful to the FAPESP for support under grant 2009/14787-7 and 2010/01490-3, respectively.

EKG and LSP acknowledge support within the framework of Sonderforschungsbereich (SFB 881) on 'The Milky Way System' (especially subproject A5), which is funded by the German Research Foundation (DFG).

OLD thanks the Universidad Nacional de La Plata where part of this work was done.

LSP and OLD thank the hospitality of the Astronomisches Rechen-Institut Heidelberg University where part of this investigation was carried out.

This work was partly funded by the subsidy allocated to Kazan Federal University for the state assignment in the sphere of scientific activities (LSP).

This research has made use of the NASA/IPAC Extragalactic Database (NED) which is operated by the Jet Propulsion Laboratory, California Institute of Technology, under contract with the National Aeronautics and Space Administration.

REFERENCES

Allende Prieto C., Lambert D. L., Asplund M., 2001, ApJ, 556, L63
Alloin D., Collin-Souffrin S., Joly M., Vigroux L., 1979, A&A, 78, 200
Alloin D., Bica E., Bonatto C., Prugniel P., 1992, A&A, 266, 117
Baldwin J. A., Phillips M. M., Terlevich R., 1981, PASP, 93, 5
Baldwin J. A., Hamann F., Korista K. T., Ferland G. J., Dietrich M., Warner C., 2003, ApJ, 583, 649
Batra N. D., Baldwin J. A., 2014, MNRAS, 439. 771
Bresolin F., Schaerer D., González Delgado R. M., Stasińska G., 2005, A&A, 441, 981
Cohen R. D., 1983, ApJ, 273, 489
Contini M., 2012, MNRAS, 425, 1205
Copetti M. V. F., Mallmann J. A. H., Schmidt A. A., Castañeda H. O., 2000, A&A, 357, 621
Dhanda N., Baldwin J. A., Bentz M. C., Osmer P. S., 2007, ApJ, 658, 804
Dors O. L., Copetti M. V. F., 2005, A&A, 437, 837
Dors O. L., Storchi-Bergmann T., Riffel R. A., Schimdt A. A., 2008, A&A, 482, 59
Dors O. L., Krabbe A. C., Hägele G. F., Pérez-Montero E., 2011, MNRAS, 415, 3616
Dors O. L., Jr, Riffel R. A., Cardaci M. V., Hägele G. F., Krabbe Á. C., Pérez-Montero E., Rodrigues I., 2012, MNRAS, 422, 252
Dors O. L. et al., 2013, MNRAS, 432, 2512
Dors O. L., Cardaci M. V., Hägele G. F., Krabbe A. C., 2014, MNRAS, 443, 1291
Du P., Wang J.-M., Hu C., Valls-Gabaud D., Baldwin J. A., Ge J.-Q., Xue S.-J., 2014, MNRAS, 438, 2828
Durret F., Bergeron J., 1988, ApJS, 75, 273
Ellison S. L., Patton D. R., Simard L., McConnachie A. W., Baldry I. K., Mendel J. T., 2010, MNRAS, 407, 1514
Ellison S. L., Patton D. R., Mendel J. T., Scudder J. M., 2011, MNRAS, 418, 2043
Fathi K., Storchi-Bergmann T., Riffel R. A., 2006, ApJ, 641, L25
Ferland G. J., Baldwin J. A., Korista K. T., Hamann F., Carswell R. F., Phillips M., Wilkes B., Williams R. E., 1996, ApJ, 461, 683
Goodrich R. W., Osterbrock D., 1983, ApJ, 269, 416
Groves B. A., Heckman T. M., Kauffmann G., 2006, MNRAS, 371, 1559
Gusev A. S., Pilyugin L. S., Sakhibov F., Dodonov S. N., Ezhkova O. V., Khramtsova M. S., 2012, MNRAS, 424, 1930
Hägele G. F., Pérez-Montero E., Díaz A. I., Terlevich E., Terlevich R., 2006, MNRAS, 372, 293
Hägele G. F., Díaz A. I., Terlevich E., Terlevich R., Pérez-Montero E., Cardaci M. V., 2008, MNRAS, 383, 209
Hamann F., Ferland G. J., 1992, ApJ, 391, L53
Hamann F., Ferland G. J., 1993, ApJ, 418, 11
Hamann F., Korista K. T., Ferland G. J., Warner C., Baldwin J., 2002, ApJ, 564, 592
Ho L. C., Filippenko A. V., Sargent W. L. W., 1997, ApJS, 112, 315
Hummer D. G., Storey P. J., 1987, MNRAS, 224, 801
Izotov Y. I., Thuan T. X., 2008, ApJ, 687, 133
Izotov Y. I., Guseva N. G., Fricke K. J., Stasińska G., Henkel C., Papaderos P., 2010, A&A, 517, 90
Kauffmann G. et al., 2003, MNRAS, 346, 1055
Kennicutt R. C., Bresolin F., Garnett D. R., 2003, ApJ, 591, 801
Kewley L. J., Dopita M. A., 2002, ApJS, 142, 35
Kewley L. J., Ellison S., 2008, ApJ, 681, 1183
Kewley L. J., Dopita M. A., Sutherland R. S., Heisler C. A., Trevena J., 2001, ApJ, 556, 121
Kewley L. J., Rupke D., Zahid H. J., Geller M. J., Barton E. J., 2010, ApJ, 721, L48

Koski A. T., 1978, ApJ, 223, 56
Krabbe A. C., Rosa D. A., Dors O. L., Pastoriza M. G., Winge C., Hägele G. F., Cardaci M. V., Rodrigues I., 2014, MNRAS, 435, 1155
Kraemer S. B., Wu C.-C., Crenshaw D. M., Harrington J. P., 1994, ApJ, 435, 171
Lauberts A., 1982, The ESO/Uppsala Survey of the ESO (B) Atlas. European Southern Observatory, Garching
Leitherer C. et al., 1999, ApJ, 123, 3
López-Sánchez Á. R., Esteban C., 2010, A&A, 517, 85
Martin P., Roy J. R., 1995, ApJ, 445, 161
Mathews W. G., Ferland G. J., 1987, ApJ, 323, 456
Matsuoka K., Nagao T., Maiolino R., Marconi A., Taniguchi Y., 2009, A&A, 503, 721
Nagao T., Murayama T., Taniguchi Y., 2001, ApJ, 549, 155
Nagao T., Maiolino R., Marconi A., 2006a, A&A, 447, 157
Nagao T., Maiolino R., Marconi A., 2006b, A&A, 447, 863
Osterbrock D. E., 1981, ApJ, 249, 462
Osterbrock D. E., Dahari O., 1983, ApJ, 273, 478
Osterbrock D. E., Ferland G., 2006, Astrophysics of Gaseous Nebulae and Active Galactic Nuclei, 2nd edn. University Science Books, Mill Valley, CA
Pagel B. E. J., Edmunds M. G., Blackwell D. E., Chun M. S., Smith G., 1979, MNRAS, 189, 95
Peimbert M., 1967, ApJ, 150, 825
Pérez-Montero E., Contini T., 2009, MNRAS, 398, 949
Pérez-Montero E., Díaz A. I., 2003, MNRAS, 346, 105
Pérez-Montero E., Hägele G. F., Contini T., Díaz A. I., 2007, MNRAS, 381, 125
Pettini M., Pagel B. E. J., 2004, MNRAS, 348, L59
Phillips M. M., Charles P. A., Baldwin J. A., 1983, ApJ, 266, 485
Pilyugin L. S., 2000, A&A, 362, 325
Pilyugin L. S., 2001, A&A, 369, 594
Pilyugin L. S., 2003, A&A, 399, 1003
Pilyugin L. S., Thuan T. X., 2005, ApJ, 631, 231
Pilyugin L. S., Vílchez J. M., Contini T., 2004, A&A, 425, 849
Pilyugin L. S., Thuan T. X., Vílchez J. M., 2006, MNRAS, 367, 1139
Pilyugin L. S., Thuan T. X., Vílchez J. M., 2007, MNRAS, 376, 353
Pilyugin L. S., Grebel E. K., Mattsson L., 2012, MNRAS, 424, 2316
Pilyugin L. S., Lara-López M. A., Grebel E. K., Kehrig C., Zinchenko I. A., López-Sánchez Á. R., Vílchez J. M., Mattsson L., 2013, MNRAS, 432, 1217
Pilyugin L. S., Grebel E. K., Kniazev A. Y., 2014, AJ, 147, 131
Pilyugin L. S., Grebel E. K., Zinchenko I. A., 2015, MNRAS, 450, 3254
Prieto M. A., Marco O., Gallimore J., 2005, MNRAS, 364, L28
Radovich M., Rafanelli P., 1996, A&A, 306, 97
Richardson C. T., Allen J. T., Baldwin J. A., Hewett P. C., Ferland G. J., 2014, MNRAS, 437, 2376
Riffel R. A., Storchi-Bergmann T., Winge C., McGregor P. J., Beck T., Schmitt H., 2008, MNRAS, 385, 1129
Riffel R., Rodríguez-Ardila A., Aleman I., Brotherton M. S., Pastoriza M. G., Bonatto C., Dors O. L., 2013a, MNRAS, 430, 2002
Riffel R. A., Storchi-Bergmann T., Winge C., 2013b, MNRAS, 430, 2249
Rosa D. A., Dors O. L., Krabbe A. C., Hägele G. F., Cardaci M. V., Pastoriza M. G., Rodrigues I., Winge C., 2014, MNRAS, 444, 2005
Rubin R. H., 1989, ApJS, 69, 897
Rupke D. S. N., Kewley L. J., Barnes J. E., 2010, ApJ, 710, L156
Sánchez S. F. et al., 2014, A&A, 563, 49
Schmitt H. R., Storchi-Bergmann T., Baldwin J. A., 1994, ApJ, 423, 237
Schnorr-Müller A., Storchi-Bergmann T., Riffel R. A., Ferrari F., Steiner J. E., Axon D. J., Robinson A., 2011, MNRAS, 413, 149
Schnorr-Müller A., Storchi-Bergmann T., Nagar N. M., Robinson A., Lena D., Riffel R. A., Couto G. S., 2014, MNRAS, 437, 1708
Shuder J. M., 1980, ApJ, 240, 32
Shuder J. M., Osterbrock D. E., 1981, ApJ, 250, 55
Storchi-Bergmann T., Schmitt H. R., Calzetti D., Kinney A. L., 1998, AJ, 115, 909 (SB98)
Storchi-Bergmann T., Dors O. L., Jr, Riffel R. A., Fathi K., Axon D. J., Robinson A., Marconi A., Östlin G., 2007, ApJ, 670, 959
Thuan T. X., Pilyugin L. S., Zinchenko I. A., 2010, ApJ, 712, 1029
Tremonti C. A. et al., 2004, ApJ, 613, 898
van Zee L., Salzer J. J., Haynes M. P., O'Donoghue A. A., Balonek T. J., 1998, AJ, 116, 2805
Viegas S. M., 2002, Rev. Mex. Astron. Astrofis., 12, 219
Vila-Costas M. B., Edmunds M. G., 1992, MNRAS, 259, 121
Wang J.-M. et al., 2011, ApJ, 739, 3
Zaritsky D., Kennicutt R. C., Huchra J. P., 1994, ApJ, 420, 87
Zhang Z. T., Liang Y. C., Hammer F., 2013, MNRAS, 430, 2605

This paper has been typeset from a TEX/LATEX file prepared by the author.